NASA
Technical
Paper
2124

January 1983

Mechanics of Liquid Helium in a Partially Filled Rotating Dewar in Low Gravity - With Application to Gravity Probe-B

C. F. Schafer
and S. A. Lowry

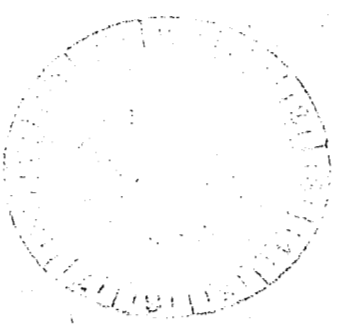

NASA

NASA
Technical
Paper
2124

1983

Mechanics of Liquid Helium in a Partially Filled Rotating Dewar in Low Gravity - With Application to Gravity Probe-B

C. F. Schafer
and S. A. Lowry
George C. Marshall Space Flight Center
Marshall Space Flight Center, Alabama

NASA
National Aeronautics
and Space Administration

**Scientific and Technical
Information Branch**

ACKNOWLEDGMENTS

The authors wish to express their thanks to George Fichtl and Fred Leslie, Atmospheric Science Division, Fluid Dynamics Branch, for helpful discussions of fluid physics relevant to the Gravity Probe-B liquid helium dewar, and to Gene Urban, Astrophysics Division, Infrared Astronomy Branch, for discussions of the physics of superfluid helium.

TABLE OF CONTENTS

LIST OF ILLUSTRATIONS

LIST OF ILLUSTRATIONS (Concluded)

TECHNICAL PAPER

MECHANICS OF LIQUID HELIUM IN A PARTIALLY FILLED ROTATING DEWAR IN LOW GRAVITY – WITH APPLICATION TO GRAVITY PROBE-B

INTRODUCTION

The Gravity Probe-B (GP-B) spacecraft (Fig. 1) is designed to test the Equivalence Principle through long-term (1 year) monitoring of forces on a set of gyros in free-fall around the Earth. Extraneous forces on these gyros must be kept at very low levels, corresponding to accelerations of 10^{-10} g or less. This will require a drag-free (to 10^{-10} g) control system, which uses a proof mass similar to the experiment gyros as its sensing element. In addition, the measurement system for monitoring these low force levels will require cooling to below superconducting transition temperatures. The approaches to both cooling and control involve the use of liquid helium. The boil-off from the liquid helium dewar will be used as a propellant to maintain the drag-free operation of the spacecraft. The requirement for an operational lifetime approaching one year means that a large quantity of liquid helium must be used, and that it will be gradually depleted over the experiment lifetime. This varying amount of liquid helium gives rise to the possibility of several problems which can degrade the GP-B experiment. Most of these potential problems are due to asymmetry in the static liquid helium distribution or to waves in the free surface which will be present in the partially-filled dewar. Before discussing these problems in detail, however, it must be determined whether classical fluid mechanics applies to the analyses. This determination is necessary because of the variety of unusual effects observed in liquid helium at low temperatures.

FLUID MECHANICS OF LIQUID HELIUM

Helium exists in nature as a mixture of two isotopes, He^4 and He^3. The relative abundance of the He^3 is only about one part in 10^6, however [1]. Helium can then for most purposes be considered to consist of He^4 only. This isotope, when in a liquid state, has two phases called HeI and HeII. Figure 2 [2] is the low temperature phase diagram for He^4 (helium). There is a phase transition line, called the λ-line, which separates the liquid HeI and liquid HeII phases. The terminus of this line on the gas-liquid line is called the λ-point. This denotes the temperature at which the HeI-HeII transition occurs at saturated vapor pressure conditions. This temperature is 2.172°K.

Liquid HeI is found to behave normally. That is, experiments on liquid HeI exhibit properties and phenomena which are common to viscous fluids. The theory which describes this behavior is classical fluid mechanics. Liquid HeII (i.e., liquid helium below 2.172°K) is found experimentally to exhibit behavior which cannot be explained classically. Some of the properties observed are:

1) The fountain effect. This effect is the flow of liquid helium through capillaries (or through pores) from colder to hotter regions.

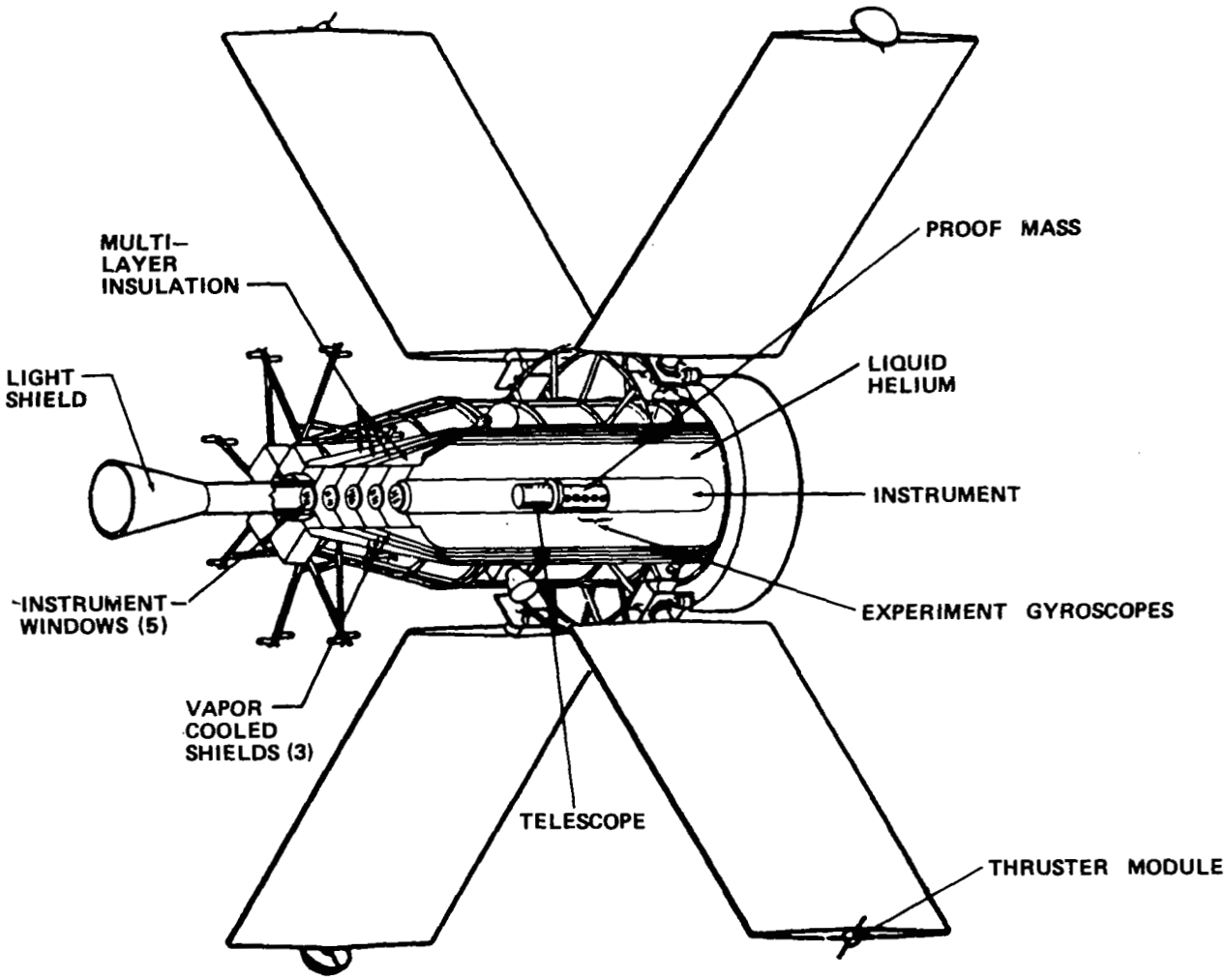

Figure 1. Gravity Probe-B.

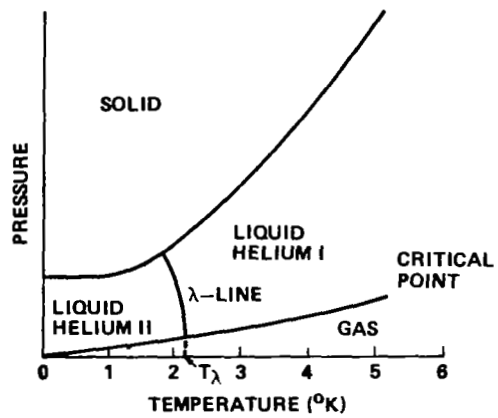

Figure 2. Low temperature phase diagram for He^4.

2) The mechano-caloric effect. This is the inverse of the fountain effect. Here, when liquid helium flows through porous material from one reservoir to another, the reservoir which is losing material experiences a rise in temperature.

3) Ability to flow through narrow regions such as slits and capillaries without sustaining a drop in pressure. This effect disappears above some critical opening size and some critical velocity. The opening size and velocity critical values are dependent on each other.

4) Related to this last effect, in experiments involving the rotation of liquid helium in geometries below critical size and at subcritical velocities, the liquid helium is seen to only partially contribute to the moment of inertia of the container. At the λ-point, all the liquid helium participates in the rotation, but at lower temperatures, the measured moment of inertia of the container and liquid helium decreases as a function of temperature. Interpretation of these results requires a two-fluid model of liquid helium involving a normal viscous component and a superfluid component.

For the GP-B spacecraft liquid helium management problem, the geometries are so large that the critical values will be exceeded. The liquid helium is treated, then, as a normal viscous fluid (with a very low viscosity, on the order of 15 micropoise). This has been experimentally verified for large containers by Mason, et al. [3]. The laws and methods of classical fluid mechanics will therefore apply here.

GP-B EXPERIMENT CONFIGURATION

The planned configuration for GP-B is shown in Figure 1. The region of the spacecraft dewar containing the liquid helium is nearly an annular volume between concentric cylinders. In discussing liquid helium configuration and dynamics that is the model which will be used (Fig. 3). The helium liquid and gas will be assumed to occupy the annular region of length 294 cm, outer radius 54 cm, and inner radius 18 cm.

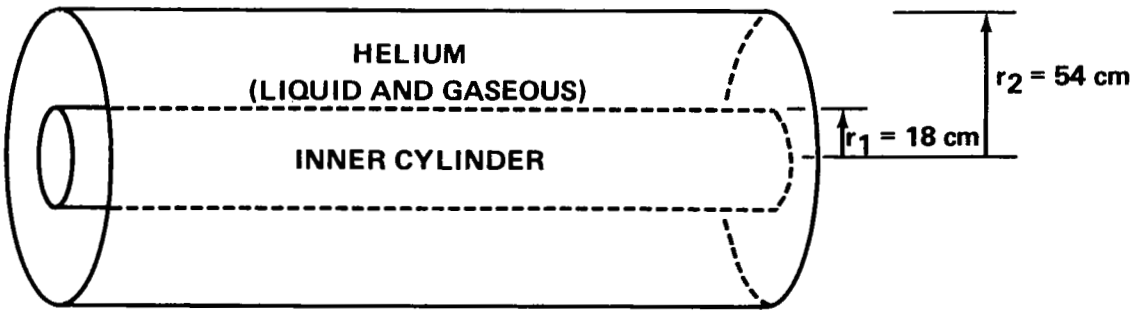

Figure 3. GP-B model system.

LIQUID HELIUM CONFIGURATION

The requirement that accelerations experienced by the proof mass be kept at the 10^{-10} g level or lower means that the liquid helium used for cooling and propulsion can be a source of problems for the GP-B system. The proof mass responds to external forces as the sensing portion of the drag compensation system. When the proof mass experiences external forces, the gaseous helium propulsion system responds with thrusts which will null net forces to the 10^{-10} g level or lower. If the forces on the proof mass are due to spacecraft drag, then the desired effect is achieved. If the forces are from other sources such as gravitation, then the effects of accelerating the spacecraft can still null net forces on the proof mass, but not on the experimental gyros since the effects of the gravitational forces will vary over the spacecraft. Also the effect of accelerating the reference frame (the spacecraft) to compensate for a force internal to the frame will result in orbital changes for the spacecraft.

In order for the GP-B drag compensation system to function properly, internal forces must be kept below the 10^{-10} g design requirement.

Gravitational forces can perturb the proof mass if there are distributions of liquid helium which are not both axially symmetric and longitudinally symmetric about a plane containing the center of mass and perpendicular to the rotation axis. Liquid helium distributions lacking these symmetries will result in gravitational effects on the proof mass in two different ways. First, the unsymmetric liquid helium distribution will have a mutual attraction with the proof mass. If we consider worst case mass distributions, we can establish upper bounds on these gravitational attractions. For the dewar half full, and with all the liquid helium at one end, the gravitational acceleration produced at the proof mass is of the order of 10^{-9} g or the dewar half full, with the liquid helium on one side, the resulting acceleration level at the proof mass is about 10^{-8} g (see Appendix A).

The second problem introduced by unsymmetric liquid helium mass distributions is the gravity gradient effect. Distributions of liquid helium which lack the proper symmetry (as described above) will cause the center of mass of the spacecraft to shift away from the center of the proof mass. The path of the proof mass in orbit will then be slightly different than that followed by the spacecraft center of mass. The force on the proof mass resulting from this nonfree-fall trajectory can be computed by expanding the expression for the Earth's gravitational attraction about the spacecraft center of mass. After doing this, we find that the magnitude of accelerations due to this effect at the proof mass can be of the order of 10^{-9} g or greater for worst case mass distributions (see Appendix B).

We have established that unsymmetric distributions of liquid helium can result in acceleration levels at the proof mass which can be more than two orders of magnitude above experiment design requirements. Whether or not these distributions can arise depends on the balance of forces acting on the liquid helium. Forces which must be considered are:

1) Spacecraft drag

2) Spacecraft propulsion

3) Gravity gradient forces

4) Gravitational forces between the liquid helium and the spacecraft

5) Centrifugal forces due to spacecraft rotation

6) Surface tension forces in the liquid helium.

For a spacecraft operating as designed, spacecraft drag will be balanced by the helium propulsion system. There should be no net accelerations (above the 10^{-10} g level) on the liquid helium from these sources. In Appendix C, the expected magnitudes of gravitational, gravity gradient, centrifugal, and surface tension forces on the liquid helium are compared. Gravity and gravity gradient forces are shown to be at least one order of magnitude smaller than the smallest expected centrifugal forces. For purposes of discussing the liquid helium configuration then, spacecraft drag and propulsion and gravity and gravity gradient forces can be neglected. To a close approximation the liquid helium configuration will be the result of a balance between centrifugal forces and surface tension for the boundary conditions imposed by dewar shape.

When the GP-B spacecraft is deployed it will not be spinning. In the early stages of the experiment, a spin rate of up to about 0.1 rad/sec will be imposed for instrument calibration. After calibration, the rotation rate will be reduced to its operational value of approximately 0.01 rad/sec. Changes in rotation rate of the spacecraft are not felt immediately in the liquid helium. Angular momentum must be diffused and convected into the liquid helium from the side and ends of the dewar. Until the helium is in solid body rotation with the spacecraft, pressure distributions due to centrifugal forces will deviate from hydrostatic and will be unpredictable. Appendix D deals with this problem. It is shown there that spin-up times are very short (a day) compared to experiment lifetime.

Knowing that equilibrium configurations of the liquid helium are governed by the centrifugal force-surface tension balance, and that spin-up can be accomplished fairly rapidly, permits analyses which can make some predictions about expected configurations. These analyses use two approaches, energy analysis and pressure balance.

Energy analyses are used to predict whether, for a given set of conditions, a simply connected ("spherical") bubble of gaseous helium or a multiply connected ("toroidal") bubble is expected. Appendices E and F deal with this approach. Results show that for the operational rotation rate, and for high fill factors (small bubble volumes), conditions are marginal for forming the desired toroidal bubble. That is, an unsymmetric liquid helium distribution could result from these conditions.

Pressure balance calculations have been performed in order to obtain equilibrium liquid helium distributions as a function of rotation rate and fill factor. Appendix G uses pressure balance to obtain gaseous helium bubble shapes in a longitudinal section containing the rotation axis. Here curvature is considered in the r-z plane. Appendix H assumes that an axisymmetric toroidal bubble exists, and computes equilibrium configurations as a function of rotation rate. In the calculations in Appendix H, the helium gas-liquid interface is assumed to have a finite radius of curvature only in the r-θ plane (i.e., in a plane perpendicular to the rotation axis). Results from these pressure balance computations confirm that axisymmetric liquid helium configurations are not expected for high fill factors at the operational rotation rate of 0.01 rad/sec.

CONCLUSIONS

Liquid helium mass distributions in the GP-B dewar are possible which are capable of producing accelerations on the proof mass on the order of 10^{-8} g. Since the proof mass is displaced from the

experiment masses, these accelerations cannot be compensated by the drag-free propulsion system. Also, the response of the drag-free propulsion system to these kinds of internal forces could degrade the orbital dynamics of the spacecraft. It was shown that the configuration of the liquid helium in the dewar is primarily a function of centrifugal forces and surface tension. Energy and force balance analyses indicate that at the planned operational rotation rate, the desired axisymmetric liquid helium configuration is improbable for high fill factors and marginal for lower fill factors. Approaches to achieving the symmetric distribution will be discussed in a separate report.

REFERENCES

1. Weast, Robert C. (editor): Handbook of Chemistry and Physics. 50th edition, Chemical Rubber Company, Cleveland, Ohio, 1970.

2. Donnelly, R. J.: Experimental Superfluidity. University of Chicago Press, 1967.

3. Mason, P., Collins, D., Petrac, D., Yang, L., Edeskuty, F., Schuch, A., and Williamson, K.: The Behavior of Superfluid Helium in Zero Gravity. Proc. 7th International Cryogenic Engineering Conference, Surrey, England, Science and Technology Press, 1978.

APPENDIX A

WORST CASE MASS DISTRIBUTIONS AND THEIR EFFECTS

Worst Case Longitudinal Displacement of GP-B Center of Mass

The worst case GP-B center of mass displacement due to an asymmetrical configuration of the liquid helium will exist if the dewar is half full and all the liquid helium is at one end (Fig. A-1).

GASEOUS HELIUM	LIQUID HELIUM
GASEOUS HELIUM	LIQUID HELIUM

Figure A-1. Worst case – axial.

Assuming a total dry mass M_1 of the dewar to be 1921.8 kg, the mass M_2 of liquid helium (for completely filled dewar) to be 320.5 kg, and the dewar length to be 294 cm, the center of mass displacement along the axis for this worst case is given by:

$$\Delta L_{c.m.} = \frac{M_1(0)}{M_1 + M_2} + \frac{M_2\,(294/4)}{M_1 + M_2}$$

$$= \frac{(160.25)\,(73.5)}{1921.8 + 160.25}\ \text{cm}$$

$$= 5.66\ \text{cm} \quad .$$

Worst Case Radial Displacement of GP-B Center of Mass

The worst case of center of mass displacement in a radial direction for the GP-B will occur if the dewar is half full and all the liquid helium is at one side (Fig. A-2).

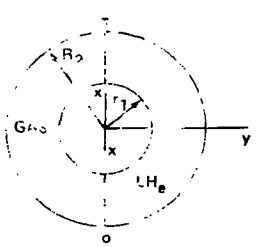

Figure A-2. Worst case – radial.

Assuming a uniform mass density, ρ, of liquid helium, the location of the helium center of mass will be given by:

$$X_{c.m.} = \frac{\rho \int_{r_1}^{r_2} dr \int_0^{\pi} d\theta \, (r^2 \cos\theta)}{\rho \int_{r_1}^{r_2} dr \int_0^{\pi} d\theta \, (r)} = \sin\theta \Big|_0^{\pi} f(r) = 0$$

$$Y_{c.m.} = \frac{\rho \int_{r_1}^{r_2} dr \int_0^{\pi} d\theta \, (r^2 \sin\theta)}{\rho \int_{r_1}^{r_2} dr \int_0^{\pi} d\theta \, (r)}$$

$$= -\cos\theta \Big|_0^{\pi} \left\{ \frac{(r^3/3) \Big|_{r_1}^{r_2}}{\pi (r^2/2) \Big|_{r_1}^{r_2}} \right\}$$

$$= \frac{4}{3\pi} \frac{(r_2^3 - r_1^3)}{(r_2^2 - r_1^2)}$$

for $r_1 = 18$ cm and $r_2 = 53$ cm

$$Y_{c.m.} = \left(\frac{4}{3\pi}\right) \left(\frac{(53)^3 - (18)^3}{(53)^2 - (18)^2}\right)$$

$$= 24.43 \text{ cm} \quad .$$

This value of the liquid helium center of mass displacement gives a radial displacement of the total GP-B center of mass of:

$$\Delta R_{c.m.} = \frac{M_1(0)}{M_1 + M_2} + \frac{M_2\,(Y_{c.m.})}{M_1 + M_2}$$

$$= \frac{(160.25)\,(24.43)}{1921.8 + 160.25}\ \text{c.m.} = 1.88\ \text{cm} \quad .$$

Gravitational Attraction Between the Proof Mass and the Liquid Helium

The displacement of the liquid helium center of mass from the spacecraft center of mass (hence from the proof mass center of mass) results in gravitational attraction between the liquid helium and the proof mass. This can be expressed as an acceleration at the proof mass location due to the liquid helium:

$$a = \frac{GM}{r^2}$$

where M is the liquid helium mass and r is the distance between the proof mass and liquid helium centers of mass.

The maximum center of mass displacements for a half full dewar have been calculated. For the longitudinal case this results in the following acceleration level:

$$a_L = \frac{GM}{r^2} = \frac{(6.67 \times 10^{-8})\,(1.60 \times 10^{5})}{(7.35 \times 10^{1})^2}\ \text{cm/sec}^2$$

$$= 1.98 \times 10^{-6}\ \text{cm/sec}^2 = 2.02 \times 10^{-9}\ \text{g} \quad .$$

For the case where the dewar is half full with all the liquid helium at one side:

$$a_R = \frac{(6.67 \times 10^{-8})\,(1.60 \times 10^{5})}{(2.443 \times 10^{1})^2}\ \text{cm/sec}^2$$

$$= 1.79 \times 10^{-5}\ \text{cm/sec}^2 = 1.83 \times 10^{-8}\ \text{g} \quad .$$

APPENDIX B

GRAVITY GRADIENT EFFECTS

The acceleration due to the gravitational attraction of the Earth at a point on an orbiting spacecraft may be expressed as an expansion about the spacecraft center of mass :

$$\bar{a}_g = - GM \frac{\hat{R}}{|\bar{R}|^2} \quad ,$$

where G is the gravitational constant, M is the mass of the Earth, and R is a vector from the center of the Earth to a point on the spacecraft. Now let

$$\bar{R} = \bar{R}_1 + \bar{R}_2 = (R_e + h)\,\hat{R}_1 + \bar{R}_2 \quad ,$$

where $\bar{R}_1$ is the vector from the center of the Earth to the spacecraft center of mass, $\bar{R}_2$ is the vector from the spacecraft center of mass to the point in question, R_e is the radius of the Earth, and h is the spacecraft altitude (Fig. B-1).

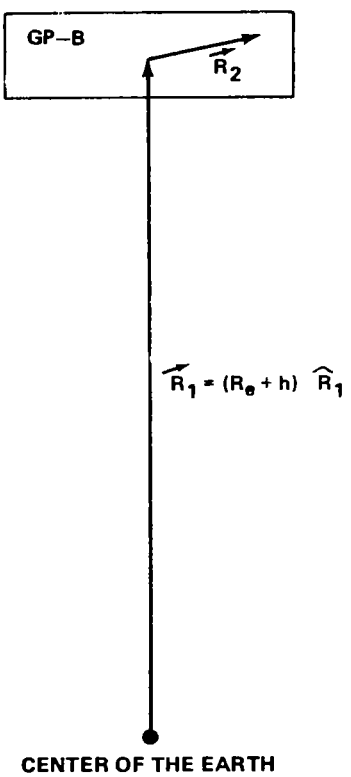

Figure B-1. Gravity gradient.

Also,

$$\hat{R} = \frac{\bar{R}}{|\bar{R}|} = \frac{\bar{R}_1 + \bar{R}_2}{|\bar{R}|} \quad .$$

We can then write:

$$\bar{a}_g = - GM \frac{\bar{R}_1 + \bar{R}_2}{|\bar{R}|^3} = \frac{\bar{R}_1 + \bar{R}_2}{[\bar{R} \cdot \bar{R}]^{3/2}}$$

or

$$\bar{a}_g = - GM (\bar{R}_1 + \bar{R}_2) [(\bar{R}_1 + \bar{R}_2) \cdot (\bar{R}_1 + \bar{R}_2)]^{-3/2}$$

$$= - GM (\bar{R}_1 + \bar{R}_2) [R_1^2 + 2 \bar{R}_1 \cdot \bar{R}_2 + R_2^2]^{-3/2}$$

$$= - GM (\bar{R}_1 + \bar{R}_2) \left[R_1^2 \left(1 + 2 \frac{\bar{R}_1 \cdot \bar{R}_2}{R_1^2} + \frac{R_2^2}{R_1^2} \right) \right]^{-3/2}$$

$$= - GM (\bar{R}_1 + \bar{R}_2) \left(\frac{1}{R_1^3} \right) \left[1 + 2 \frac{\hat{R}_1 \cdot \bar{R}_2}{R_1} + \frac{R_2^2}{R_1^2} \right]^{-3/2} \quad .$$

This can be expanded in a binomial series. If we wish to have accuracy to the third power of $1/R_1$, we need to retain only the first two terms in the expansion. We have then:

$$\bar{a}_g \cong - GM \left(\frac{\hat{R}_1}{R_1^2} + \frac{\bar{R}_2}{R_1^3} \right) \left[1 - 3 \frac{\hat{R}_1 \cdot \bar{R}_2}{R_1} \right] \quad .$$

Again keeping terms through $1/R_1^3$,

$$\bar{a}_g \cong - GM \left[\frac{\hat{R}_1}{R_2^2} - 3 \frac{\hat{R}_1 \cdot \bar{R}_2}{R_1^3} \hat{R}_1 + \frac{\bar{R}_2}{R_1^3} \right] \quad .$$

We observe that the first term is just the gravitational acceleration at the spacecraft center of mass. This term is balanced by the centrifugal acceleration of the spacecraft. For a spacecraft in an inertial flight mode, the second and third terms represent unbalanced accelerations. The result will be that a mass at any point away from the spacecraft center of mass experiences gravity gradient forces. The component of displacement perpendicular to the radius generates forces directed back toward the center of mass. The component of displacement along the radius r_1 generates forces away from the center of mass.

For GP-B, then, if there is any displacement of the spacecraft center of mass from the proof mass center of mass, gravity gradient forces will act on the proof mass in the manner described above. Any distribution of liquid helium lacking axial symmetry (including symmetry about a plane perpendicular to the axis and through the proof mass) will cause these forces. It is useful to make worst case estimates of the magnitude of these effects.

If $\bar{R}_2$ is taken to be a vector to a point fixed in the GP-B spacecraft, and is assumed to lie in the orbital plane, then the angle between $\bar{R}_1$ and $\bar{R}_2$ can be represented by $\omega t + \phi$ where ω is the orbital angular rate, t is the time, and ϕ is a fixed place angle. If we take $\phi = 0$ for the angle at which R_1 and R_2 are aligned, and let $t = 0$ at that point, then we have:

$$\hat{R}_1 \cdot \bar{R}_2 = |\bar{R}_2| \cos \omega t \quad .$$

The gravity gradient part of the acceleration can then be written:

$$\bar{a} \cong - GM \left[- 3 \frac{R_2}{R_1^3} \cos \omega t \, \hat{R}_1 + \frac{\bar{R}_2}{R_1^3} \right]$$

$$= - GM \left[- 3 \frac{R_2}{R_1^3} \cos \omega t \, \hat{R}_1 + \hat{R}_2 \right]$$

when $\bar{R}_2$ is parallel to $\bar{R}_1$:

$$\bar{a}(0) = - GM \frac{R_2}{R_1^3} [- 2 \hat{R}_1]$$

where $\bar{R}_2$ is antiparallel to $\bar{R}_1$:

$$\bar{a}(\pi) = - GM \frac{R_2}{R_1^3} [2 \hat{R}_1] \cdot$$

When $\bar{R}_2$ is perpendicular to $\bar{R}_1$, i.e., cos $\omega t = 0$, we have:

$$\bar{a}(\pi/2) = \bar{a}(3\pi/2) = - GM \frac{R_2}{R_1^3} [\hat{R}_2] \quad .$$

Examination of these expressions for gravity gradient acceleration shows that it is directed toward the center of mass of the spacecraft for $\hat{r}_1 \perp \hat{r}_2$, and away from the center of mass for $\bar{r}_1$ parallel to $\bar{r}_2$, and has maximum magnitudes of $2GMR_2/R_1^3$. Where:

$G = 6.67 \times 10^{-8}$ cm^3 gm^{-1} sec^{-2}

M = mass of Earth = 5.98×10^{27} gm

$R_1 = Re + h$

R_e = radius of Earth = 6.37×10^8 cm

h = altitude = 520 km = 5.2×10^7 cm

a = gravity gradient acceleration

$= 2(6.67 \times 10^{-8}) (5.98 \times 10^{27}) (R_2)/(6.89 \times 10^8)^3$

$= 2.44 \times 10^{-6} R_e$ sec^{-2} $= 2.49 R_2 \times 10^{-9}$ g ,

where R_2 must be expressed in cm, and represents the amount of center of mass displacement due to asymmetries in the helium configuration.

APPENDIX C

FORCES ON LIQUID HELIUM

Gravity Gradient Accelerations

From Appendix B, the expression for the gravity gradient acceleration at a point represented by the vector R_2 from the spacecraft center of mass is given by:

$$\vec{a} \cong - GM_e \left[\frac{\bar{R}_2}{R_1^3} - 3 \frac{\hat{R}_1 \cdot \bar{R}_2}{R_1^3} \right] \quad .$$

An estimate of the magnitude of this acceleration was shown to be:

$$a \cong 2.5 \, R_2 \times 10^{-9} \text{ g} \quad ,$$

where R_2 is expressed in centimeters. For R_2 = 150 cm,

$$a \cong 4 \times 10^{-7} \text{ g} \quad .$$

Gravitational Accelerations

The gravitational acceleration everywhere inside the GP-B dewar can be determined in principle as:

$$\vec{a}(\vec{r}) = - \overline{\nabla} \, \phi(\bar{r}) \quad ,$$

where $\phi(\vec{r})$ is the gravitational potential:

$$\phi(\vec{r}) = \int_V \frac{\rho(\vec{r'})}{|\bar{r} - \bar{r}'|} \, d^3 r' \quad .$$

Here $\rho(\vec{r'})$ is the mass distribution of the spacecraft.

To determine whether it is necessary to evaluate this integral, we may obtain an estimate of $\vec{a}(\vec{r})$. An upper bound on the magnitude of $\vec{a}(\vec{r})$ will be given by assuming all the mass of the spacecraft

is concentrated at the center of mass and computing the acceleration at a distance L/2 away, where L is the dewar length. For L = 150 cm, and M (the spacecraft mass) to be 1900 kg, we have :

$$a = \frac{G\,M}{r^2}$$

$$= \frac{(6.67 \times 10^{-8}\ \text{cm}^3\ \text{gm}^{-1}\ \text{sec}^{-2})\ (1.9 \times 10^{6}\ \text{gm})}{(1.5 \times 10^{2})^2}$$

$$= 5.63 \times 10^{-6}\ \text{cm/sec}^2$$

$$= 5.74 \times 10^{-9}\ \text{g} \quad .$$

Surface Tension Forces

The pressure difference across any fluid-fluid interface (Fig. C-1) is given by:

$$\Delta P = \sigma \left(\frac{1}{R_1} + \frac{1}{R_2} \right) \quad ,$$

where σ is the interfacial tension measured as a force per unit length, and R_1 and R_2 are the principal radii of curvature at a point on the interface.

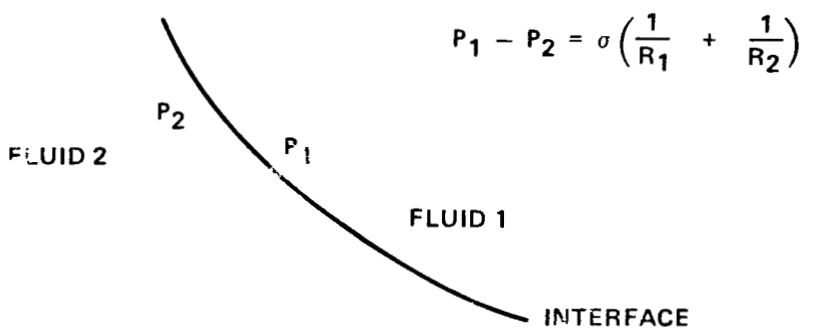

Figure C-1. Pressure across 2-fluid interface.

For liquid helium various values for σ have been reported. A value on the upper end of the range is 0.53 dynes/cm [1]. Other values range downward to about 0.12 [3]. Using σ = 0.53 dynes/cm and a characteristic radius of 18 cm (the inner cylinder radius for GP-B), we obtain ΔP = 0.029 dynes/cm^2. A pressure can be calculated which would result from a hydrostatic head due to an acceleration field of 4×10^{-7} g (the value derived as an upper limit of gravity gradient effects). This would be

$$P = \rho\, g\, h = (0.145\ \text{gm/cm}^3)\ (4 \times 10^{-4}\ \text{cm/sec}^2)\ (54\ \text{cm})$$

$$= 0.0031\ \text{dynes/cm}^2 \quad ,$$

where the radius of the GP-B dewar provides the 54 cm length scale.

This value is a factor of 10 smaller than the surface tension forces. We can expect then that surface tension will be much more important than gravity gradient effects in determining liquid helium configuration.

Centrifugal Forces

Since the GP-B spacecraft will rotate about its longitudinal axis, the liquid helium in the dewar will experience centrifugal forces. The acceleration field due to this rotation is given by :

$$a_c = \omega^2 r \quad ,$$

where ω is the rotation rate. At the operational rotation rate of about 0.01 rad/sec, we have :

$$a_c = 10^{-4}\ r \quad .$$

Expressed in effegravity this becomes :

$$a_c \cong 10^{-7}\ r\ g \quad ,$$

where r is in centimeters.

For r = 18, $a_c = 1.8 \times 10^{-6}$ g and for r = 54, $a_c = 5.4 \times 10^{-6}$ g. These levels are about an order of magnitude higher than the largest expected gravitational effects and comparable to surface tension effects.

APPENDIX D

SPIN-UP AND SPIN-DOWN OF THE GP-B

A fluid in a container undergoing a uniform rotation about a single axis will ultimately come into equilibrium with the container and the container-fluid system will rotate as a solid body. When this condition is achieved, a hydrostatic pressure distribution exists in the fluid. The pressure distribution may readily be computed from the centrifugal force and is just a function of distance from the rotation axis, fluid density, and rotation rate. When the fluid is not spun-up, that is when it is adjusting to a changing angular velocity of the container, the pressure distribution is very complex. In order to have an experimental condition which is known, it is preferable for the liquid helium in the GP-B dewar to be spun-up while the experiment is being conducted. It is necessary then to compute estimates of the time required for the liquid helium to adjust to changing angular velocities. This characteristic time will be denoted as the spin-up time.

The model appropriate for the GP-B dewar is concentric cylinders with the liquid helium contained in the annular region between them (Fig. D-1). The problem then is to get angular momentum (vorticity) into the liquid helium from the rotating cylinders. There are two transport processes available to carry this vorticity generated at the container walls (see W. B. Watkins, R. G. Hussey, Spin-up from rest in a cylinder, Physics of Fluids, Vol. 20, No. 10, Pt. 1, Oct. 1977). First, vorticity generated at the walls of the dewar diffuses into the liquid helium. The characteristic time for this process is $\tau_d \approx a^2/\nu$, where a is the radius of the outer cylinder and ν is the kinematic viscosity of the liquid helium. For a = 53.34 cm and for $\nu = \mu/\rho$ = dynamic viscosity/density = $(1.3 \times 10^{-6}$ poise$)/0.1452$ gm/cm^3 = 8.95×10^{-5} cm^2/sec, we have a characteristic time:

$$\tau_d = (53.34 \text{ cm})^2/8.95 \times 10^{-5} \text{ cm}^2/\text{sec}$$

$$= (28.45 \times 10^2)/8.95 \times 10^{-5} \text{ sec}$$

$$= 3.18 \times 10^7 \text{ sec} = 368 \text{ days} \approx 1 \text{ year} \quad .$$

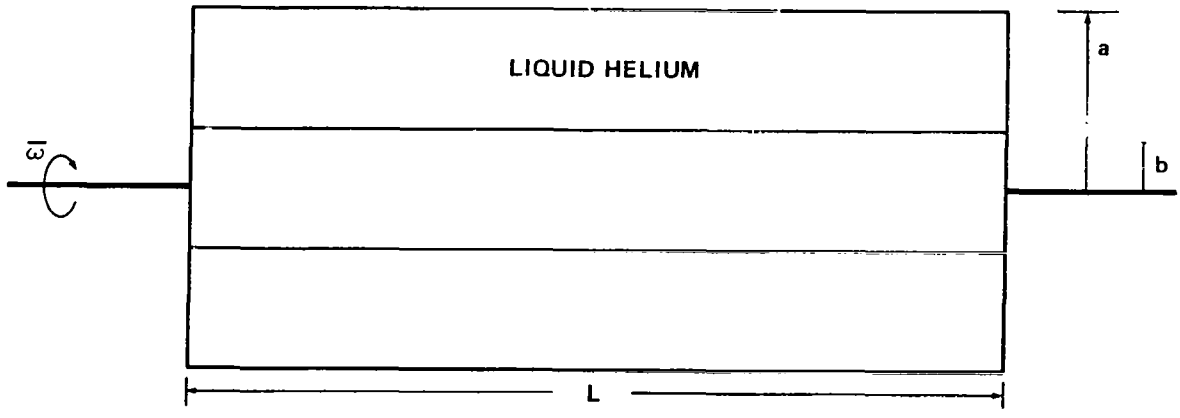

Figure D-1. Spin-up model.

Spin-up through diffusion of viscosity from the walls is then a very slow process, requiring a time of the order of the experiment lifetime to occur. The second process which contributes to spin-up is the convective transport of vorticity due to centrifugal pumping (Eckman pumping) at the cylinder end walls. Figure D-2 indicates the nature of this effect. Liquid in contact with the end wall must rotate at the angular rate, w, of the end wall. Shear stresses in the viscous liquid entrains a layer having thickness the order of $\delta = (\nu/w)^{1/2}$ (see H. P. Greenspan, The Theory of Rotating Fluids, Cambridge Univ. Press, 1968, p. 32). Here $\delta = (8.95 \times 10^{-5}\ cm^2/sec)/10^{-2}\ rad/sec^{1/2} = 9.5 \times 10^{-2}$ cm, that is, δ is about 1 millimeter. The fluid in this layer has angular velocity and therefore is subject to centrifugal forces which push it radially outward. The sidewalls turn the flow. For a closed cylinder where there is centrifugal pumping at each end, toroidal flow cells develop, extending from each end to the midplane of the cylinder. The spin-up time scale due to this mechanism is given by:

$$\tau_c = L(\nu\omega)^{-1/2}$$

where L is the cylinder length. For L = 294 cm this gives:

$$\tau_c = (294\ cm)\ (8.95 \times 10^{-5}\ cm^2/sec)\ (10^{-2}\ rad/sec)^{-1/2}$$

$$= 3.12 \times 10^5\ sec = 3.61\ days\ .$$

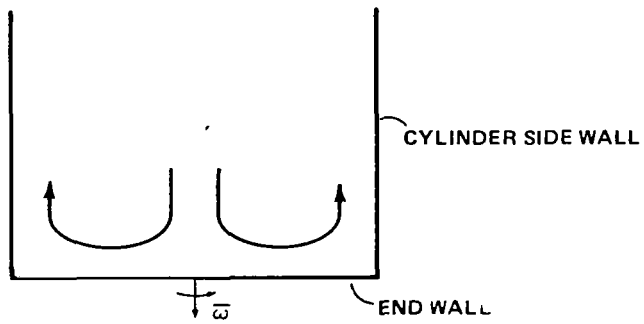

Figure D-2. End wall effects.

Since the spin-up time is directly proportional to the length scale L, a decrease in this time may be obtained by making L smaller. This could be done by using baffles which would be plates parallel to the cylinder ends. Then the characteristic length would be the baffle spacing. If this spacing is about L/10, then the characteristic spin-up time reduces to about 1/3 day.

Since $\tau_c \ll \tau_d$, the spin up will be completely dominated by centrifugal pumping. τ_c is short enough that hydrostatic conditions should be established quickly (compared to total experiment time).

Spin-down occurs in a fluid by the same mechanisms as spin-up. Therefore, reductions in rotation rate for GP-B will be accomplished through the end wall pumping effects, and will have the same characteristic time as for spin-up.

APPENDIX E

ENERGY ANALYSIS

Given a vapor bubble of specified volume, we will eventually be concerned with its position both along the axis and in the radial direction. However, for the time being, ignore the bubble's position along the axis and consider only its radial position. For the case where the cylinder is not rotating, the bubble might look like Figure E-1. As long as the bubble was small enough to fit between the cylinders, its shape would be spherical. (Note that liquid helium at this temperature is a perfectly wetting liquid thus preventing the bubble from attaching and forming a solid-vapor interface.) With zero rotation, the radial position of this vapor bubble would be arbitrary, but with even a slight rotation the bubble would begin to float toward the center of the container as the heavier liquid was forced toward the outside (Fig. E-2).

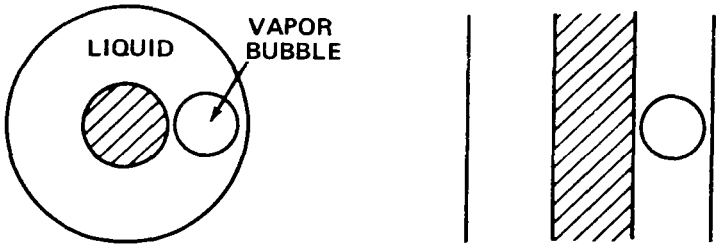

Figure E-1. Bubble in nonrotating case.

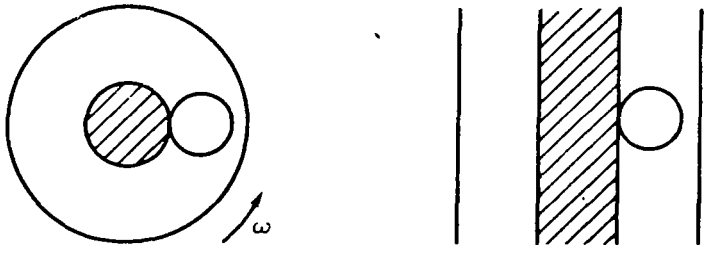

Figure E-2. Bubble with small ω.

When the bubble reaches the inner cylinder its final shape depends on a combination of factors. Those parameters which will affect the bubble's shape and bubble size for a given container include the density difference between the vapor and liquid phases, the vapor pressure, the surface tension of the vapor liquid interface, and the rotation rate. When the rotation rate is small relative to the surface tension, the bubble would look something like Figure E-3. However, as the rotation rate increases (or the surface tension decreases) the bubble will deform, wrapping itself around the cylinder as in Figure E-4. This deformation would continue with increased rotation until the two ends of the bubble touch. At that time the bubble would "pop" and reform into a toroidal shape (Fig. E-5).

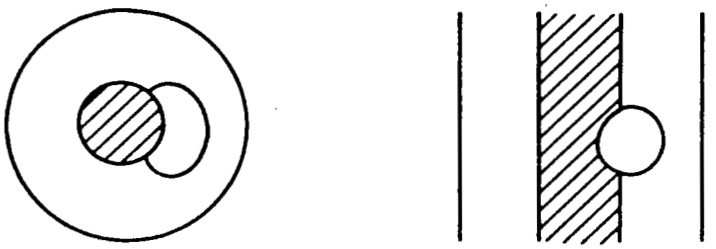

Figure E-3. Bubble with ω increasing.

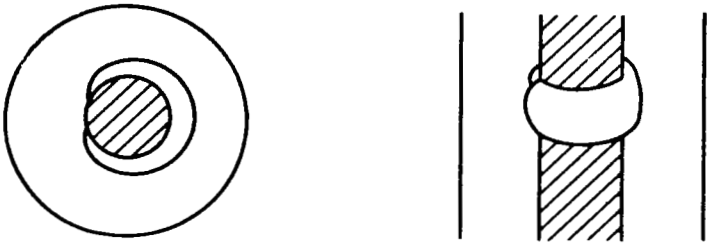

Figure E-4. Bubble, large ω.

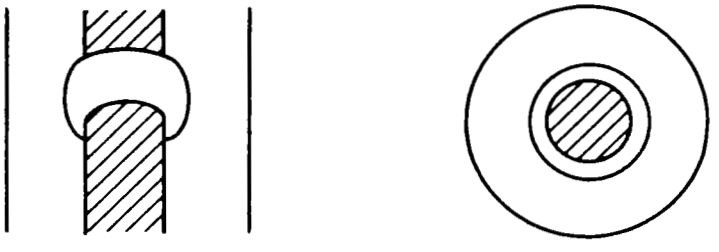

Figure E-5. Axisymmetric bubble.

It is easy to imagine that if we then slowed the rotation rate, the vapor would remain in some torus-like form, perhaps even until the cylinder stopped rotating completely. The significance is that for one rotation rate there may be two very different possible states, one axisymmetric and one not. Which shape is thermodynamically preferred depends on the balance between the surface energy and the potential energy due to rotation. The surface energy would be minimized by a spherical bubble off to one side while the potential energy due to rotation would be minimized by a bubble wrapped around the inner cylinder. Unfortunately, it is extremely difficult to calculate the actual shapes of these two states and to subsequently compare their energy. Instead we have chosen to simplify the problem by comparing the energy difference between the undistorted shapes of a sphere and a torus. The question then is what is the energy required to go from a torus to a sphere (Fig. E-6).

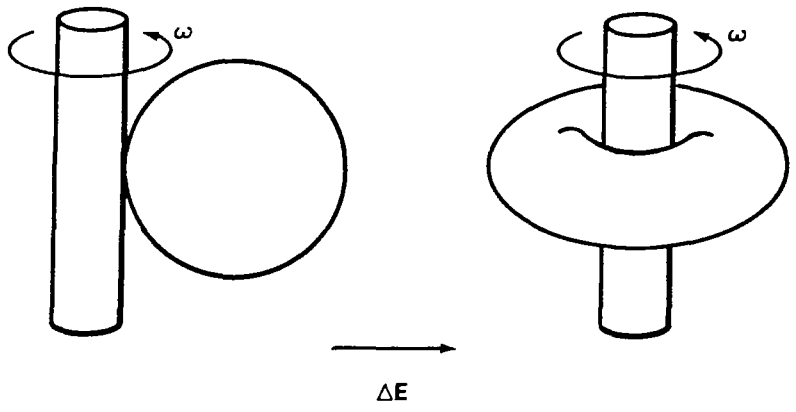

Figure E-6. Energy model.

The change in energy in going from a torus to a sphere of the same volume is the sum of the energy released by the decrease in surface area plus the energy required to transport the liquid helium through the acceleration field to its new position. (The energy required to relocate the vapor is neglected.) The first part of this sum is easily calculated and is simply $\sigma(A_S - A_T)$ where σ is the surface tension, A_S is the surface area of the sphere, and A_T is the surface area of the torus. The final result is that the difference in energy between a torus and a sphere is:

$$\Delta E_{TOTAL} = \sigma(A_T - A_S) + \omega^2 \rho \pi \left[\left(4\pi b^3(R_1 + b)\left[R_1 + \frac{7}{8} b\right]\right) - \left(\frac{14}{15} a^5 + R_1 \frac{4}{3} a^4\right)\right]$$

(Torus → Sphere)

where

σ = surface tension

A_T = area of the torus

A_S = surface area of the sphere

ω = rotation rate (radians/sec)

ρ = density (g/cm^3)

b = small radius of the torus

R_1 = radius of the inner cylinder

a = radius of the sphere .

If ΔE is positive for a given bubble volume and ω then the bubble would rather be a sphere. If E is negative then a torus is the preferred configuration. A value of $\Delta E = 0$ implies that the bubble is at a crossover point where it would just as soon be a torus as a sphere.

In order to get a feel for what shape might be expected, some examples have been worked for helium in the dewar with the dimensions shown in Figure E-7.

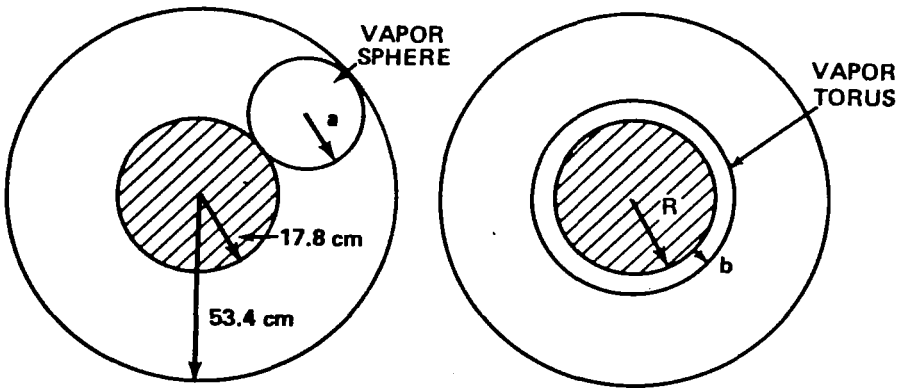

Figure E-7. Energy model with GP-B parameters.

Using the values of σ = 0.37 erg , ρ = 0.145 g/cm^3, R_1 = 17.8 cm, and ω = 0.01 rad/sec, a bubble with a volume of 24 liters (1/100 of the available volume of the actual dewar) would rather be spherical (ΔE = 975 dynes/cm). However, an increase to a rotation above 0.38 rad/sec would mean that the bubble would prefer to be a torus ($\Delta E \leqslant 0$). Similarly, a vapor bubble with a volume of 510 liters at a rotational speed of 0.01 rad/sec would rather be toroidal, but if slowed down to below W = 0.0089 would prefer to be a sphere except that such a large sphere could not fit undistorted in the space between the inner and outer cylinder.

The conclusion of this energy analysis is that near a rotation speed of 0.01 rad/sec (the projected rotation rate for the actual experiment) it is questionable what form the bubble will take.

APPENDIX F

SURFACE ENERGY AND ROTATIONAL POTENTIAL ENERGY

A slightly different energy argument from that of Appendix G is presented here. Two possible configurations of the liquid helium will be analyzed with respect to surface energy and rotational potential energy. These configurations are an axisymmetric LHe distribution (Fig. F-1) and a simply connected bubble (Fig. F-2) of helium gas. The simply connected bubble may or may not extend the length of the dewar.

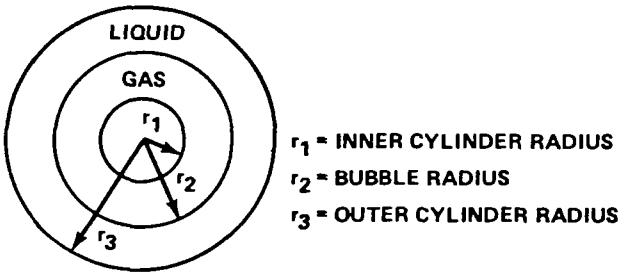

Figure F-1. Axisymmetric bubble.

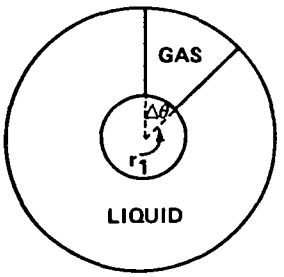

Figure F-2. Simply connected bubble.

The configuration with the lowest possible rotational potential energy is just that shown in Figure F-1. In this configuration, all the potential energy has been converted to rotational kinetic energy. Ignoring the contribution of the helium gas (which is negligible due to its very low density of the order of 10^{-3} times the LHe density), the rotational kinetic energy of this configuration is

$$E_R = \int_{\theta=0}^{2\pi} \int_{z=0}^{\ell} \int_{r_2}^{r_3} \frac{1}{2} \rho\, r^2\, \omega^2\, dV$$

$$= \frac{1}{4} \pi\, \ell\, \rho\, \omega^2\, (r_3^4 - r_2^4) \quad ,$$

where ℓ is the length of the dewar. To obtain the rotational potential energy of any configuration, we must find the difference between the rotational kinetic energy of that state and E_R.

The total energy of a given configuration will be the sum of its rotational potential energy and its surface energy. Surface energy is just:

$$E_s = \sigma A \ ,$$

where A is the total interfacial area. The total energy is then:

$$E_T = E_s + E_{potential}$$

$$= \sigma A + E_R - E_R' \ ,$$

where E_R' is the rotational kinetic energy of the given state.

For an axisymmetric bubble, the surface energy E_s^C is:

$$E_s^C = \sigma \, 2\pi \, r_2 \, \ell \ .$$

The total energy for this configuration, E_T^C is then:

$$E_T^C = E_s^C + E_R - E_R' \ .$$

Here, however, $E_R = E_R'$ so that for the axisymmetric (cylindrical) configuration:

$$E_T^C = 2\pi \, r_2 \, \ell \, \sigma \ .$$

For the simply connected bubble (which will be labeled "spherical") shown in Figure F-2, the rotational kinetic energy is:

$$E_R^S = \int_0^{\Delta\theta} \int_h^{\ell} \int_{r_1}^{r_3} \frac{1}{2} \rho \, r^2 \, \omega^2 \, dV + \int_{\Delta\theta}^{2\pi} \int_0^{\ell} \int_{r_1}^{r_3} \frac{1}{2} \rho \, r^2 \, \omega^2 \, dV \ .$$

Evaluating this integral gives:

$$E_R^s = \frac{1}{8} \rho \omega^2 (r_3^4 - r_1^4) [2\pi\ell - \Delta\theta h] \quad ,$$

where h is the length of the gas bubble and $\Delta\theta$ is its angular extent.

The rotational potential energy of this configuration is then:

$$E_{potential} = E_R - E_R^s$$

$$= \frac{1}{4} \pi \ell \rho \omega^2 (r_3^4 - r_2^4) - E_R^s$$

$$= \frac{1}{4} \pi \ell \rho \omega^2 (r_1^4 - r_2^4) + \frac{1}{8} \Delta\theta \, h \rho \omega^2 (r_3^4 - r_1^4) \quad .$$

The surface energy of this configuration is :

$$E_s^s = \sigma A = \sigma \left[2(r_2 - r_1) h + \frac{1}{2} a \Delta\theta (r_3^2 - r_1^2) \right] \quad ,$$

where

a = 1 for bubble stuck to end

a = 2 for bubble away from end .

The total energy for the simply connected bubble is:

$$E_T^s = E_s^s + E_R - E_R^s$$

$$= \sigma \left[2(r_2 - r_1) h + \frac{1}{2} a \Delta\theta (r_3^2 - r_1^2) \right] - \frac{1}{4} \pi \ell \rho \omega^2 (r_2^4 - r_1^4) + \frac{1}{8} \Delta\theta \, h \rho \omega^2 (r_3^4 - r_1^4).$$

The criterion for having an axisymmetric cylindrical bubble is that the energy for that state be lower than that for alternate states:

$$E_T^c < E_T^s$$

or

$$E_T^s - E_T^c > 0 \quad .$$

This condition is:

$$\sigma \left[2(r_2 - r_1)\, h + \frac{1}{2}\, a\, \Delta\theta\, (r_3^2 - r_1^2) - 2\pi\, r_2\, \ell \right] - \frac{1}{4}\, \pi\, \ell\, \rho\, \omega^2\, (r_2^4 - r_1^4)$$

$$+ \frac{1}{8}\, \Delta\theta\, h\, \rho\, \omega^2\, (r_3^4 - r_1^4) > 0 \quad .$$

This is subject to the condition that the volume of the gas bubble is constant. That is:

$$V^c = V^s$$

or

$$\pi\, \ell\, (r_2^2 - r_1^2) = \frac{1}{2}\, (\Delta\theta\, h)\, (r_3^2 - r_1^2)$$

so that:

$$(\Delta\theta\, h) = \frac{2\pi\, \ell\, (r_2^2 - r_1^2)}{(r_3^2 - r_1^2)} \quad .$$

Assume that h is some fraction of ℓ:

$$h = b\, \ell \qquad \text{where} \qquad 0 < b \leqslant 1$$

then

$$\Delta\theta = \frac{2\pi\, (r_2^2 - r_1^2)}{b\, (r_3^2 - r_1^2)} \quad .$$

Rewriting the energy condition we have:

$$\sigma \left[2(r_2 - r_1)\, h + \left(\frac{a}{b}\right) \pi (r_2^2 - r_1^2) - 2\pi r_2 \ell \right] - \frac{1}{4} \pi \ell \rho \omega^2 (r_2^4 - r_1^4)$$

$$+ \frac{1}{4} \pi \ell \rho \omega^2 (r_2^2 - r_1^2)(r_3^2 + r_1^2) > 0$$

or

$$F = \sigma \left[2(r_2 - r_1)\, h + \left(\frac{a}{b}\right) \pi (r_2^2 - r_1^2) - 2 \pi r_2 \ell \right]$$

$$+ \frac{1}{4} \pi \ell \rho \omega^2 (r_2^2 - r_1^2)(r_3^2 - r_2^2) > 0 \quad .$$

Then, $F(r_2, a, b, \omega) > 0$ defines the region in parameter space where an axisymmetric bubble is energetically preferred. Figures F-3 and F-4 show these regions for the following parameters:

r_1 = 18 cm

r_2 = variable (set for each calculation)

r_3 = 54 cm

ℓ = 294 cm

b = a constant between 0 and 1

a = 1 or 2

ω = independent variable

ρ = 0.145 gm/cm^3

σ = 0.53 dynes/cm .

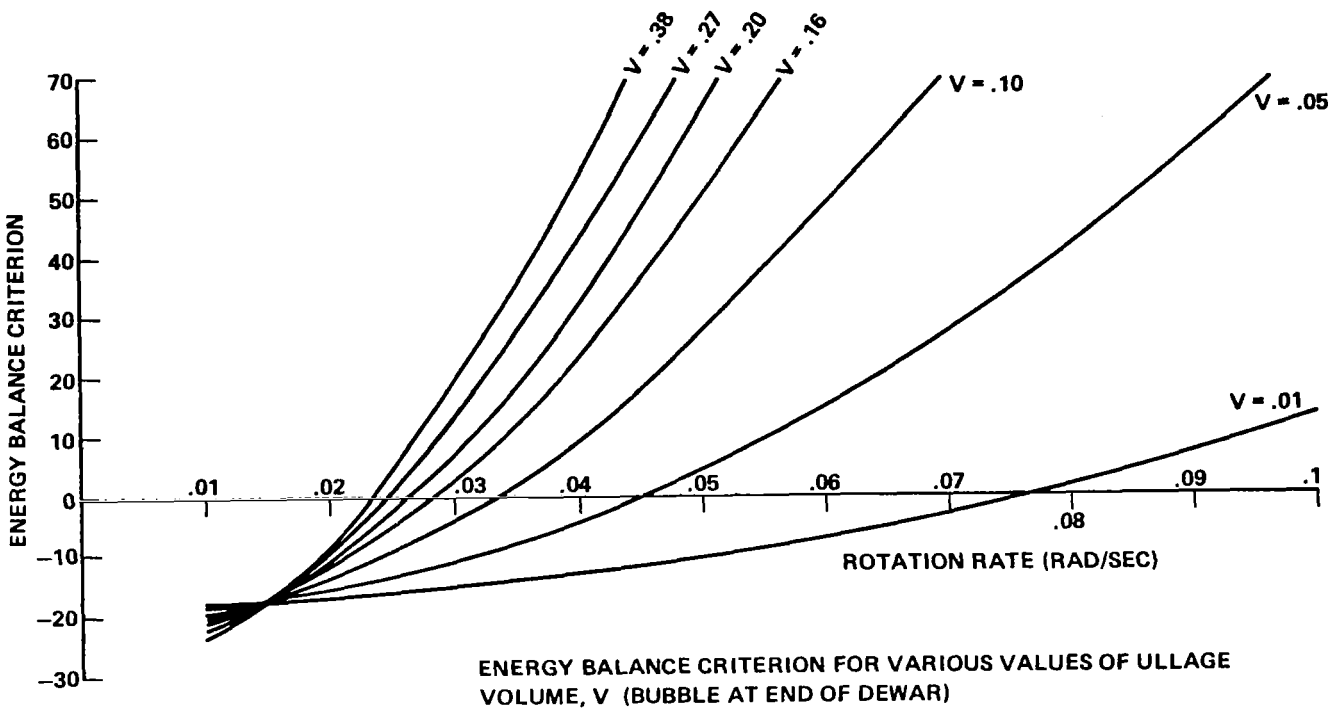

Figure F-3. Energy condition, bubble at end of dewar.

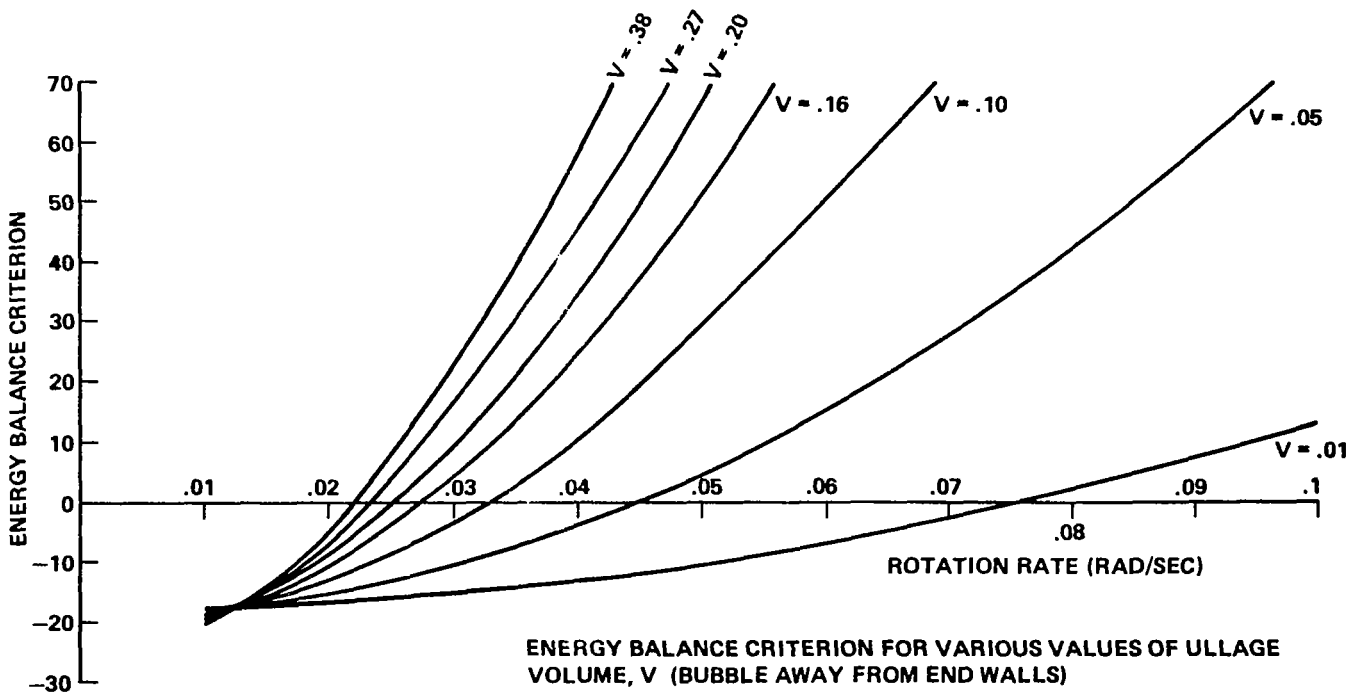

Figure F-4. Energy condition, bubble away from end of dewar.

APPENDIX G

PLOTTING THE BUBBLE SHAPE

The curvature of a bubble and therefore its shape is dictated by its surface tension and the pressure difference between the inside of the bubble and the outside. The relevant equation is:

$$\Delta P = - \sigma (K_1 \pm K_2) \quad ,$$

where ΔP is the pressure difference between the inside and outside of the bubble, σ is the surface tension and K_1 and K_2 are the orthogonal curvatures (Fig. G-1). Consider a nonrotating container of liquid helium containing a bubble of volume V (Fig. G-2). The pressure of the vapor inside the bubble is a function of the temperature. As heat flows into the container and vaporizes the liquid helium the overall temperature is held constant by means of evaporation through a porous plug. Since the temperature is fixed the vapor pressure inside the bubble likewise remains at a fixed value. The pressure in the liquid outside the bubble is then given by :

$$P_{Liquid} = - \sigma (K_1 \pm K_2) + P_{vapor} \quad .$$

For a sphere $K_1 \pm K_2 = 2/R$ where R is the radius of the sphere. Therefore for a sphere :

$$P_{liquid} = P_{vapor} - 2\sigma/R \quad .$$

Since the vapor pressure is a constant, the pressure of the liquid must increase over the course of the experiment as helium is vaporized and vented overboard (Fig. G-3).

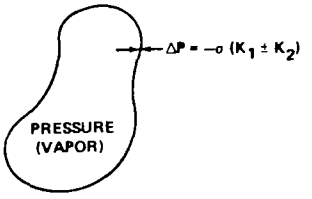

Figure G-1. Pressure drop across bubble wall.

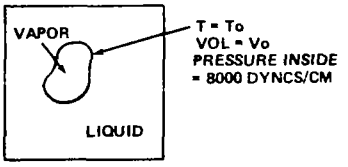

Figure G-2. Bubble in closed container.

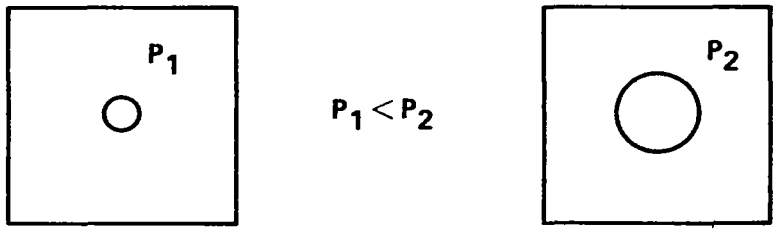

Figure G-3. Pressure change with bubble growth.

For a rotating system the problem becomes more complex but the equation $P_{liq} - P_{vap} = -\sigma\ (K_1 \pm K_2)$ still holds. For the configuration given in Figure G-2 the Navier Stokes equations in cylindrical coordinates can be applied to get an expression for the pressure in the liquid:

$$\rho\left[\frac{\partial V_r}{\partial t} + V_r\frac{\partial V_r}{\partial r} + \frac{V_\theta}{r}\frac{\partial V_r}{\partial \theta} + V_2\frac{\partial V_r}{\partial z} - \frac{V_\theta^2}{r}\right] = F_r - \frac{\partial P}{\partial r} + \mu\left[\frac{\partial^2 V_r}{\partial r^2} + \frac{1}{r}\frac{\partial V_r}{\partial r} + \frac{1}{r^2}\frac{\partial^2 V_r}{\partial \theta^2} + \frac{\partial^2 V_r}{\partial z^2} - \frac{V_r}{r^2} - \frac{2}{r^2}\frac{\partial V_\theta}{\partial \theta}\right] .$$

For the case where the fluid rotates as a solid body around the axis this equation reduces to:

$$-\rho\frac{V_\theta^2}{r} = -\frac{\partial P}{\partial r} ,$$

where ρ is the density, V_θ the velocity in the theta direction, P the pressure, and r the radial coordinate. Substituting $\omega r = V_\theta$ (where ω = radians/sec) and integrating gives:

$$\text{Pressure liquid} = \frac{\rho\,\omega^2\,r^2}{2} + \text{Constant} .$$

Substituting this expression into $P_{liq} - P_{vap} = -\sigma\ (K_1 \pm K_2)$ results in:

$$\text{Curvature } (K_1 \pm K_2) = -\frac{\rho\,\omega^2\,r^2}{2\sigma}\left[\frac{\text{Constant} + P_{Vapor}}{\sigma}\right] .$$

For a "two-dimensional bubble" $K_2 = 0$. The resulting bubble can be plotted using a computer plotting program. An example of such a bubble plot is given in Figure G-4. The figure gives an example for two different values of the constant in the above equation. The curvature for these two-dimensional bubbles with K_2 set equal to zero is sharper than would be the curvature of the cross-section of an actual bubble.

For the three-dimensional bubble which is axisymmetric (toroidal in shape) the value of $1/r$ can be substituted for K_2 again simplifying the problem where it can be easily graphed by computer. (This is an approximation for K_2 which will be exact at the inner cylinder and at the outer extremity of the bubble. The approximation should only affect the detailed shape of the bubble ends, not its size.) Figure G-5 is the side view of a torus drawn by the computer program. In the figure, S is the surface tension; ω is the rotation rate; the Int Press (8000) is the pressure of the helium vapor; and Ext Press is the pressure of the liquid helium. The bubble shown in Figure G-5 would grow as the helium was depleted and at some point would look like Figure G-6. The axial position of the bubble in Figure G-6 is for the most part arbitrary. The center of gravity of such a bubble is unpredictable and therefore undesirable. One possible remedy to this problem would be to step up the rotation rate. A higher rotation rate is more likely to produce an axisymmetric torus and will also stretch the bubble out such that at a certain volume the bubble would be positioned by the end walls. Figure G-7 shows the growth of a bubble at a higher rotation. The bubble shown in Figure G-7 would touch both end walls when its volume reached approximately one-fourth of the total volume.

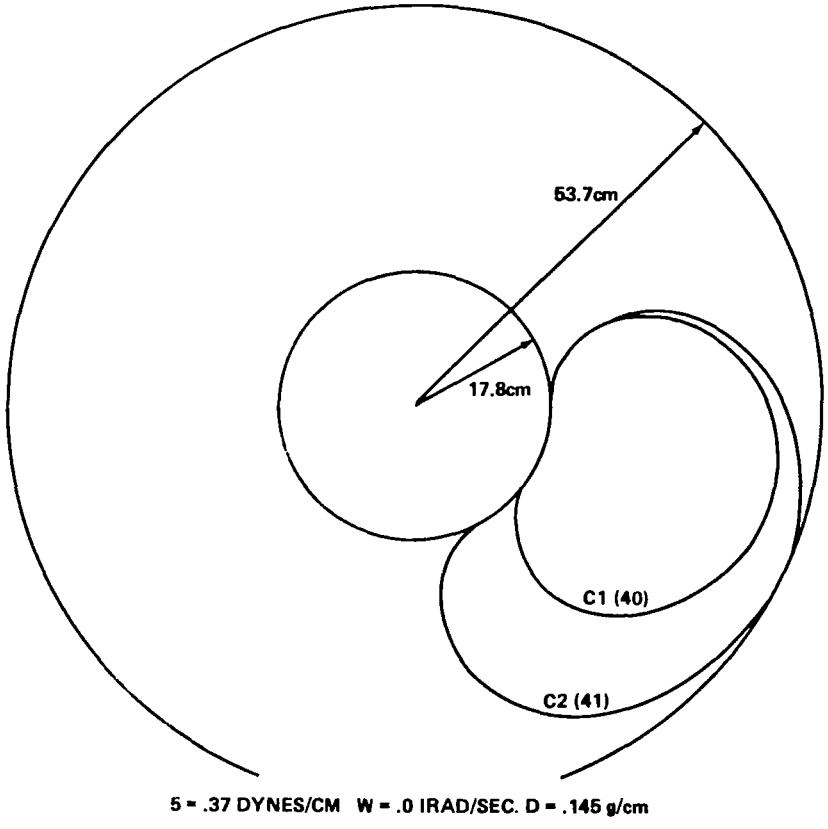

Figure G-4. Bubble shape, $r\theta$ section.

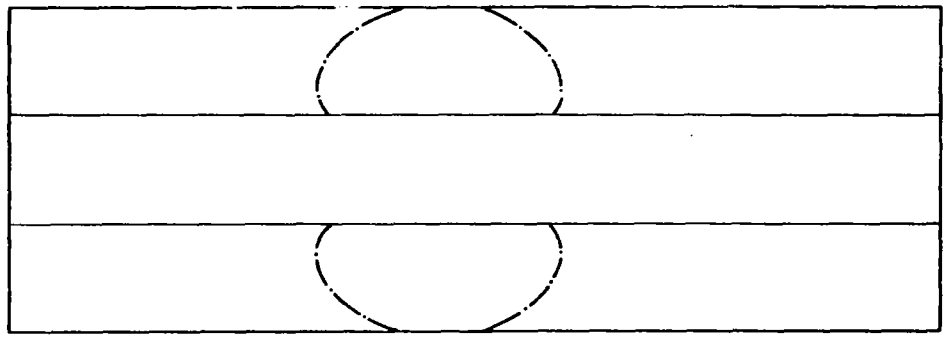

RUN #1 S = .37 dynes/cm W = .01 rad/sec. D = .145 g/cm INT PRESS = 8000 (dynes/cm^2), EXT PRESS = 7990.96548638

Figure G-5. Bubble shape, rz section.

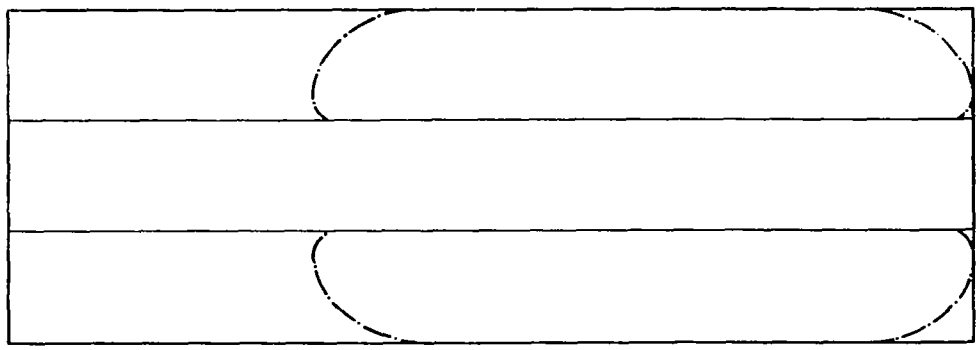

RUN #1 S = .37 DYNES/cm W = .01 RAD/SEC. D = .145 g/cm INT PRESS = 8000 (DYNES/cm^2).

Figure G-6. Bubble shape, ω = 0.01 rad/sec.

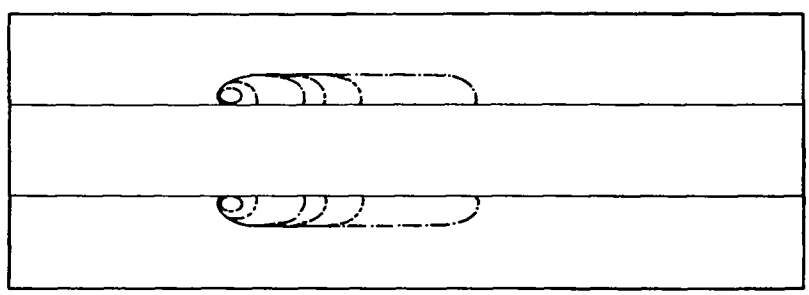

RUN #1 S = .37 dynes/cm W = .05 rad/sec. D = .145 g/cm INT PRESS = 8000 (dynes/cm^2), EXT PRESS = 7990
RUN #2 S = .37 dynes/cm W = .05 rad/sec. D = .145 g/cm INT PRESS = 8000 (dynes/cm^2), EXT PRESS = 7990.8
RUN #3 S = .37 dynes/cm W = .05 rad/sec. D = .145 g/cm INT PRESS = 8000 (dynes/cm^2), EXT PRESS = 7990.82
RUN #4 S = .37 dynes/cm W = .05 rad/sec. D = .145 g/cm INT PRESS = 8000 (dynes/cm^2), EXT PRESS = 7990.827
RUN #5 S = .37 dynes/cm W = .05 rad/sec. D = .145 g/cm INT PRESS = 8000 (dynes/cm^2), EXT PRESS = 7990.8272
RUN #6 S = .37 dynes/cm W = .05 rad/sec. D = .145 g/cm INT PRESS = 8000 (dynes/cm^2), EXT PRESS = 7990.82726
RUN #7 S = .37 dynes/cm W = .05 rad/sec. D = .145 g/cm INT PRESS = 8000 (dynes/cm^2), EXT PRESS = 7990.82726787

Figure G-7. Bubble shape, ω = 0.05 rad/sec.

APPENDIX H

CYLINDRICAL BUBBLE PRESSURE BALANCE

The pressure balance at a cylindrical interface, concentric about the rotational axis of the liquid, for the system shown in Figure H-1 is given by:

$$\sigma\left(\frac{1}{R}+0\right)=\frac{1}{2}(\rho_2-\rho_1)\,\omega^2\,(R^2-r_1{}^2)$$

or

$$\frac{2\sigma}{R}=(\rho_2-\rho_1)\,\omega^2\,R^2-(\rho_2-\rho_1)\,\omega^2\,r_1{}^2$$

$$2\sigma=(\rho_2-\rho_1)\,\omega^2\,R^3-(\rho_2-\rho_1)\,\omega^2\,r_1{}^2\,R$$

$$R^3-r_1{}^2\,R-\frac{2\sigma}{(\rho_2-\rho_1)\,\omega^2}=0\quad .$$

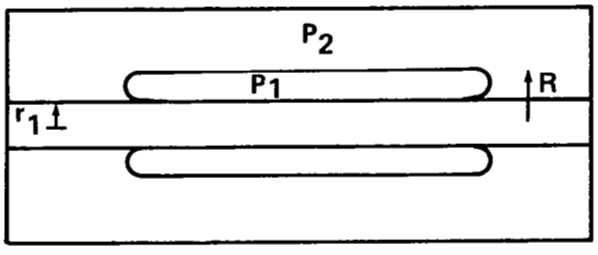

Figure H-1. Cylindrical bubble model.

This can be solved numerically to obtain R as a function of angular rate ω. R will be the radius of a cylindrical bubble which is in equilibrium at a given rotation rate. Results are shown in Figure H-2 for values of surface tension of 0.35 and 0.53 dynes/cm.

Another way to present the pressure calculations is to compute pressure drop across an interface as a function of radius of curvature of a toroidal bubble and to compare this to the pressure due to centrifugal forces at the same radius. For surface tension calculations are:

$$\Delta P=\sigma/r_2\quad .$$

For centrifugal forces, calculations are:

$$\Delta P = \frac{1}{2} (\rho_2 - \rho_1) \omega^2 (r_2^2 - r_1^2)$$

where ρ_2 = density of liquid helium and ρ_1 = density of gaseous helium. These calculations are plotted in Figures H-3 through H-5.

It is necessary to determine how full the liquid helium dewar can be at a given rotation rate and still have an axisymmetric bubble. This can be done by first finding the bubble radius consistent with equilibrium (Fig. H-2) and then determining what fill factor this represents (fill factor is 1-c, where c is the ullage fraction). Figure H-6 presents plots of ullage fraction versus bubble radius. Curve 1 of Figure H-6 represents the GP-B system as designed. Curve 2 illustrates how an axisymmetric bubble could be maintained for larger fill factors if a larger diameter dewar is used. Figure H-7 shows the ullage fraction which can be maintained at a given rotation rate assuming cylindrical bubbles.

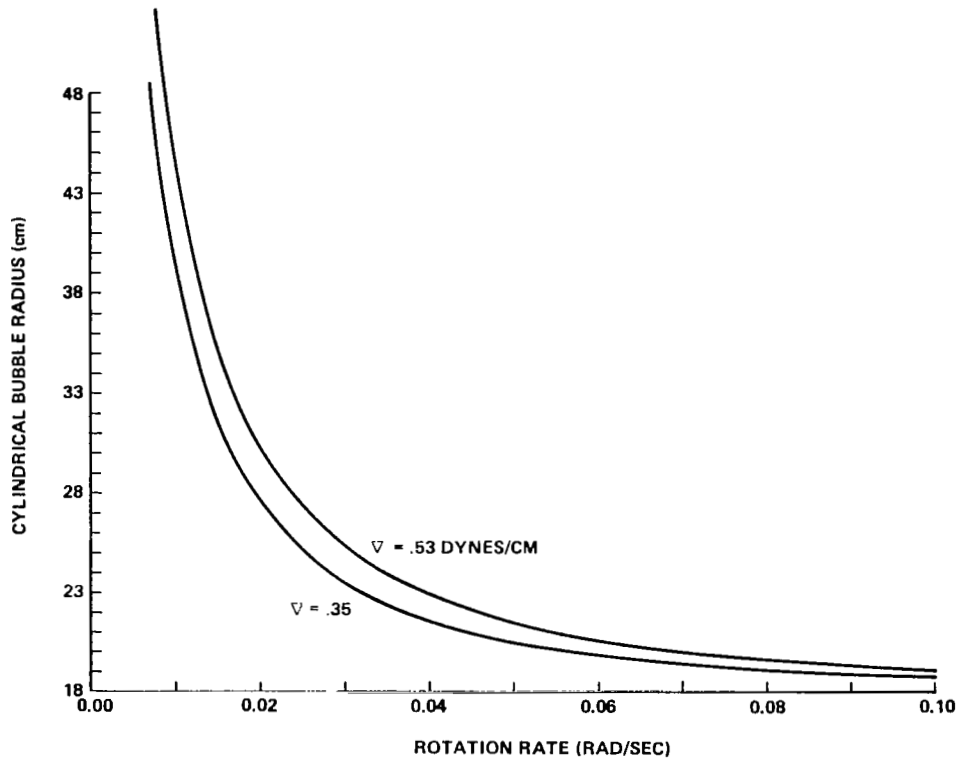

Figure H-2. Equilibrium cylindrical bubble radius versus rotation rate.

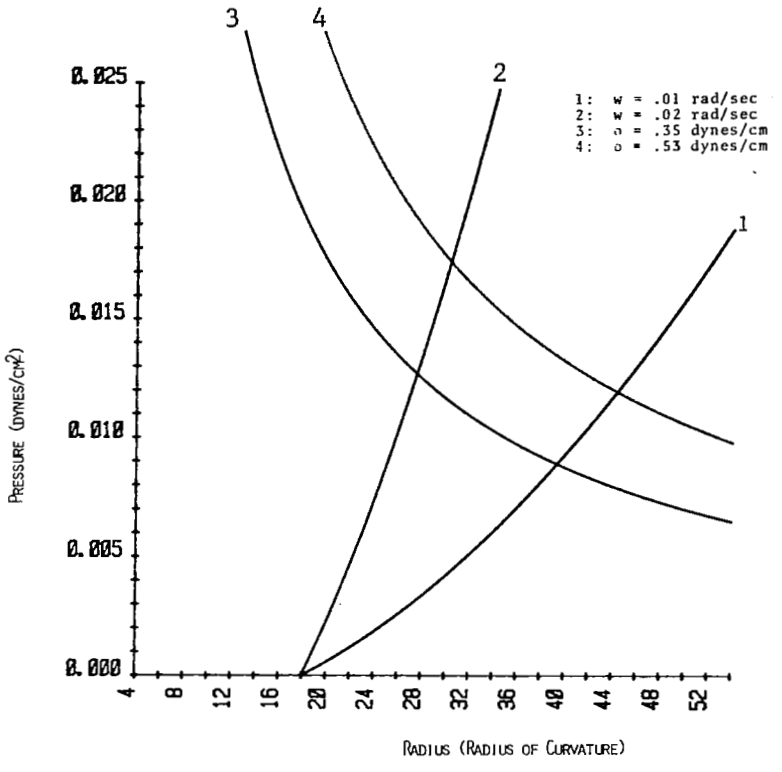

Figure H-3. Pressure versus radius of curvature for cylindrical bubble.

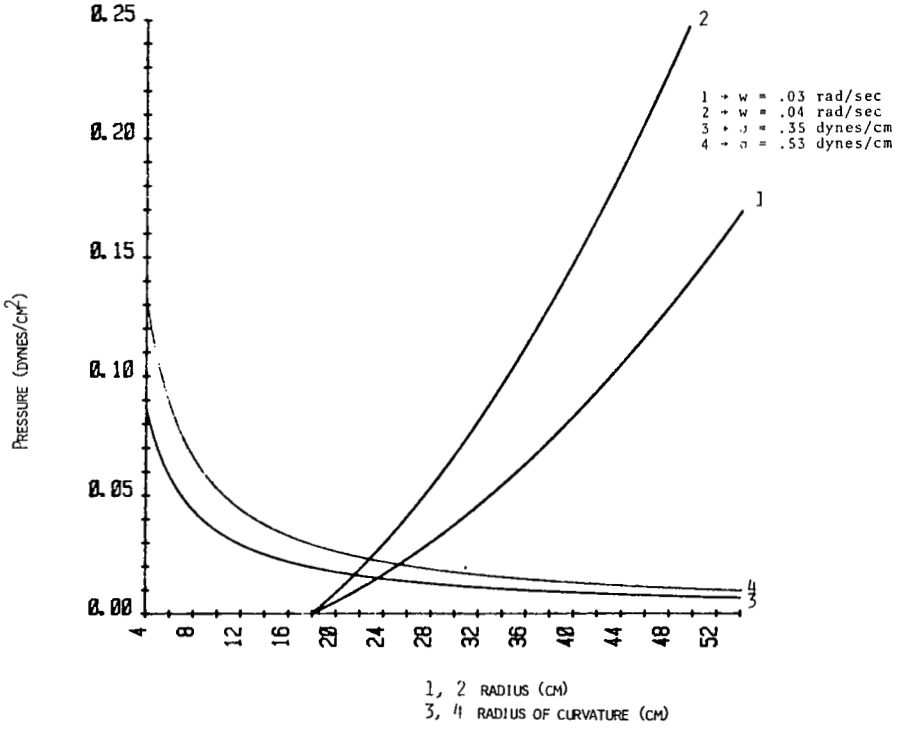

Figure H-4. Pressure versus radius of curvature for cylindrical bubble.

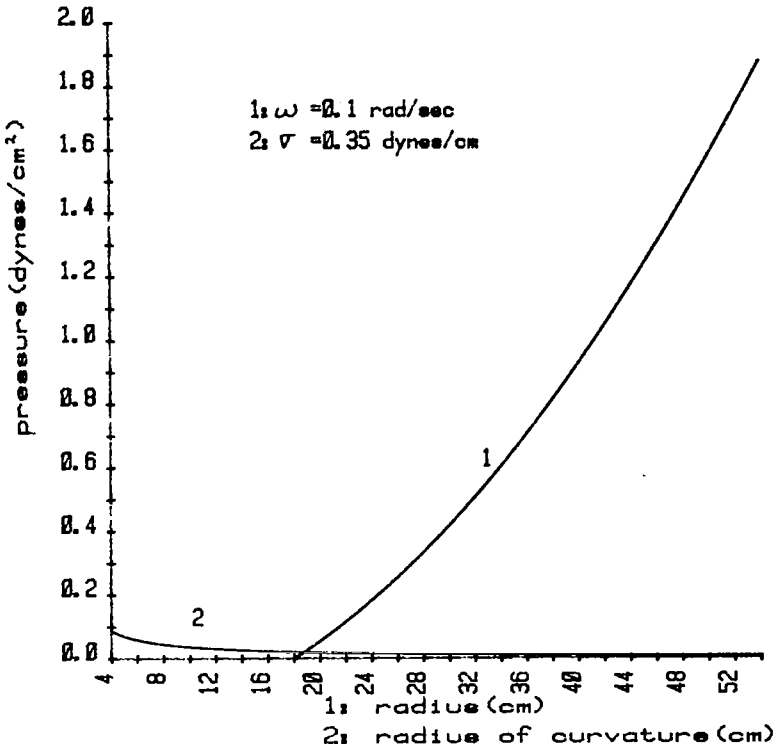

Figure H-5. Pressure versus radius of curvature for cylindrical bubble.

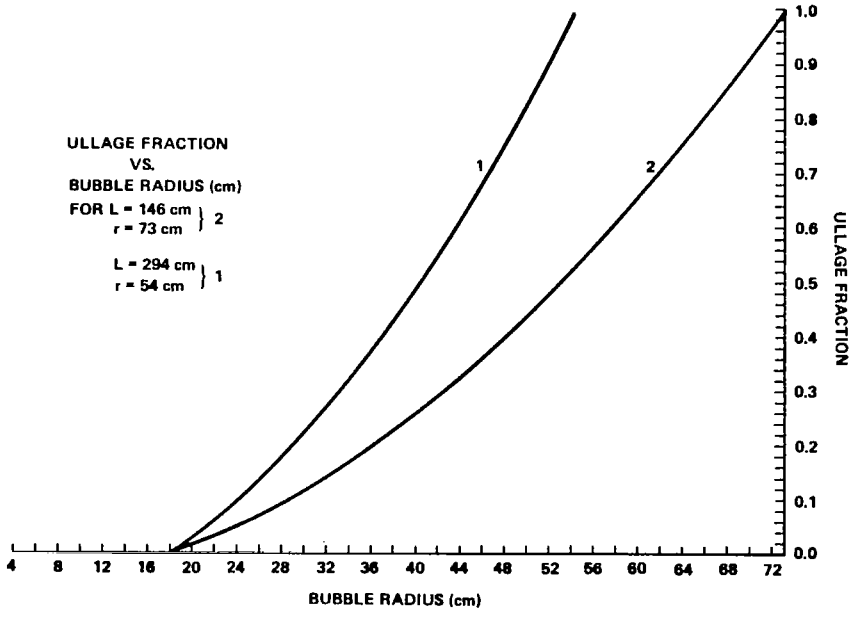

Figure H-6. Ullage fraction versus bubble radius for cylindrical bubble.

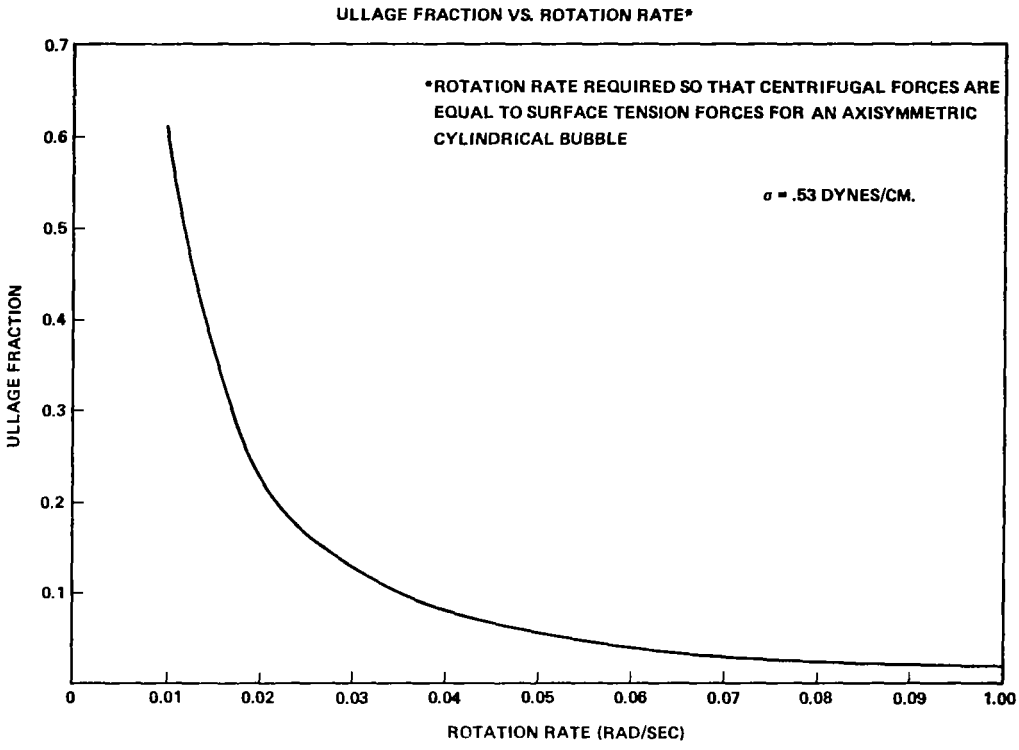

Figure H-7. Ullage fraction versus rotation rate.

1. REPORT NO.	2. GOVERNMENT ACCESSION NO.	3. RECIPIENT'S CATALOG NO.
NASA TP-2124		

4. TITLE AND SUBTITLE	5. REPORT DATE
Mechanics of Liquid Helium in a Partially Filled Rotating Dewar in Low Gravity – With Application to Gravity Probe-B	January 1983
	6. PERFORMING ORGANIZATION CODE
7. AUTHOR(S)	8. PERFORMING ORGANIZATION REPORT #
C. F. Schafer and S. A. Lowry*	
9. PERFORMING ORGANIZATION NAME AND ADDRESS	10. WORK UNIT NO.
George C. Marshall Space Flight Center Marshall Space Flight Center, Alabama 35812	M-404
	11. CONTRACT OR GRANT NO.
	13. TYPE OF REPORT & PERIOD COVERED
12. SPONSORING AGENCY NAME AND ADDRESS	Technical Paper
National Aeronautics and Space Administration Washington, D.C. 20546	14. SPONSORING AGENCY CODE

15. SUPPLEMENTARY NOTES

Prepared by Space Science Laboratory, Science and Engineering Directorate.

*Now in Structures and Propulsion Laboratory.

16. ABSTRACT

The Gravity Probe-B (GP-B) spacecraft is composed largely of a liquid helium dewar containing an experiment package. It is shown that an unsymmetric liquid helium distribution in the dewar can cause unacceptably high forces, gravitational and gravity gradient forces, at the experiment location. It is further shown that for the planned spacecraft configuration and operational parameters, it is very likely that the liquid helium distribution in the dewar will be unsymmetric. The required symmetry can be attained by using higher operational spacecraft rotation rates. An alternative solution to this problem will be discussed in a later report.

17. KEY WORDS	18. DISTRIBUTION STATEMENT
Gravity Probe-B liquid helium spacecraft dynamics	Unclassified - Unlimited Subject Category 34

19. SECURITY CLASSIF. (of this report)	20. SECURITY CLASSIF. (of this page)	21. NO. OF PAGES	22. PRICE
Unclassified	Unclassified	41	A03

For sale by National Technical Information Service, Springfield, Virginia 22151

NASA-Langley, 1983